THE JOURNAL OF PHYSICAL CHEMISTRY A

 VOLUME 107, NUMBER 34, AUGUST 28, 2003

ARTICLES

Does IVR Take Place Prior to Peptide Ion Dissociation?

Yongjun Hu,[†] Boaz Hadas,[†] Mandy Davidovitz,[†] Bülent Balta,[‡] and Chava Lifshitz*,[†]

Department of Physical Chemistry and The Farkas Center for Light Induced Processes, The Hebrew University of Jerusalem, Jerusalem 91904, Israel, and Chemistry Department, Boğaziçi University, 34342 Bebek, İstanbul, Turkey

Received: February 28, 2003; In Final Form: May 12, 2003

Small peptide ions are studied by time-resolved photodissociation (TRPD). Laser desorption of neutral peptides is combined with laser photoionization in an ion trap followed by thermalization, laser photodissociation, and time-of-flight mass analysis. Ionization and excitation take place through an aromatic chromophore at the C-terminus of the peptide, whereas dissociation produces the immonium ion at the N-terminus. The purpose is to uncover the role of intramolecular vibrational redistribution (IVR) in unimolecular fragmentations of peptide radical cations the excitation of which is site-selective. Whereas previous experiments concentrated on mass spectra, the avenue taken here is the determination of microcanonical rate constants. The rate constants are measured at a fairly well-defined internal energy E for two peptides possessing the same chromophore, undergoing the same fragmentation but having a different number of degrees of freedom. Experimental rate measurements in the range of $\sim 10^2-10^5$ s^{-1} will be presented for the peptides leucyl tyrosine (LeuTyr) and leucyl leucyl tyrosine (LeuLeuTyr). One-color (280.5 nm) two-photon ionization, thermalization for 1980 ms, and excitation at 579 nm of LeuTyr and LeuLeuTyr yield $(4.8 \pm 1.8) \times 10^3$ and $(2.9 \pm 1.9) \times 10^2$ s^{-1} inverse time constants, that is, rate constants, respectively. The rate constants provide a clear indication that the peptide length (i.e., its number of degrees of freedom) strongly correlates with the dissociation rate. This has been tested further through measurements at different photodissociation energies and through Rice−Ramsperger−Kassel−Marcus/quasi equilibrium theory (RRKM/QET) calculations that are demonstrated to be in good agreement with the experimental observations, indicating that the internal energy, E, is randomized. In other words, these peptides do not circumvent IVR.

Introduction

The theoretical treatment of mass spectral fragmentations has relied strongly on statistical theories such as Rice−Ramsperger−Kassel−Marcus/quasi equilibrium theory (RRKM/QET).[1−3] According to the QET of mass spectra, energy randomization precedes fragmentation. If during ionization an excited electronic state of the ion is reached, internal conversion will take place to the ground state of the ion and dissociation will take place from the ground state. The occurrence of so-called "isolated electronic states" that do not internally convert to the ground state before dissociation is rare.[4] As in ordinary RRKM theory of neutral molecules, intramolecular vibrational redistribution (IVR) of the energy is assumed to precede dissociation because it normally occurs on the time scale of picoseconds. The experimental examples for this behavior are numerous[1−4] and "non-RRKM" molecules are scarce. Nearly all molecules studied behave statistically (are "ergodic").

[†] The Hebrew University of Jerusalem.
[‡] Boğaziçi University.

10.1021/jp030275b CCC: $25.00
Published on Web 08/06/2003

Biomolecular ions in the gas phase are a topic of great current interest. The combination of laser desorption (LD) of neutral biomolecules, entrainment in a supersonic expansion, and laser ionization provides control over the energy deposited in the ion. In laser ionization of a neutral via a chromophore,[5] an electron is removed from a closed-shell species and cation radicals are formed. The development of mass spectrometry of biomolecules has raised again some old questions. For example, does IVR precede fragmentation? When a chromophore is locally absorbing the laser energy in one part of the peptide molecule, does the charge act as a scout to find the preferred fragmentation site leading to charge-directed and site-selective dissociation? Does electronic energy relaxation take place, or is there site selectivity and charge-directed reactivity?[6]

We have begun to answer these questions. Our major effort has been to develop a quantitative physical−chemical approach for these questions. We have constructed a unique laser desorption/laser ionization/ion trap reflectron that allows time-resolved photodissociation (TRPD) studies of peptides and determination of microcanonical rate constants, $k(E)$, as a function of energy for different series of peptides.[7] We have concentrated on cation radicals formed by laser desorption followed by laser photoionization and laser photodissociation.

We have taken upon ourselves the study of the extent of statistical versus site-selective fragmentation of small peptide radical cations. The objective was to find out to what degree does the mode of preparation of the ions and the initial site of excitation affect the type, degree, and rate of fragmentation. A major question that has been posed is as follows: Does a peptide behave as a collection of amino acids, like beads on a string,[6,8] or as a viable supermolecule, namely, an ordinary organic molecule albeit with a large number of degrees of freedom. Previous theoretical efforts coincided with some very nice experiments done on small peptides having a chromophore through which laser multiphoton ionization (MPI) and photodissociation (PD) proceed.[8] Fragmentation of these peptides has been observed as a direct outcome of the initial ionization and excitation at a specific site, followed by intramolecular charge transfer. These studies were however limited to measurements of mass spectra, and no rate−energy, $k(E)$, data were reported.

One of the major conclusions of the earlier MPI work on peptides by Weinkauf, Schlag, and co-workers[8] has been that peptides, which are not expected to fragment according to RRKM/QET on the time scale of mass spectrometry because of a very low excess energy, $E - E_0$, above the threshold E_0, do fragment because electronic excitation (or the charge) is the scout, avoiding the pitfall of large molecule kinetics. According to this conclusion, the assumption that the entire available internal energy E is distributed over all of the degrees of freedom is incorrect. The charge scouts for the site of reactivity without energy dissipation. Neither peptide length nor the number of atoms should show correlation with the dissociation observed.

We are in the process of testing this conclusion in the following way. We have studied two peptides, LeuTyr (leucyl tyrosine) and LeuLeuTyr, new experimental results for which will be reported here. Both peptides can undergo ionization at the aromatic chromophore of the C-terminus at 280.5 nm followed by thermalization and PD in the visible at 579 nm. Both undergo dissociation at the N-terminus leading to the well-known immonium ion at m/z 86 (Scheme 1). In other words, they undergo unimolecular fragmentations having the same critical energy E_0 and having nearly the same (rather small) excess energy $E - E_0$ (∼1.1−1.3 eV). Nevertheless, we will demonstrate that their microcanonical dissociation rate constants

SCHEME 1: The α-Cleavage Reaction Leading to the Immonium Ion at *m/z* 86 from the LeuTyr^{+}• Radical Cation Indicated Schematically

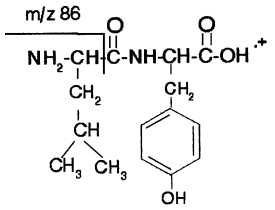

measured by the TRPD method are quite different. The two quite different rate constants provide a clear indication that the peptide length (i.e., its number of degrees of freedom) strongly correlates with the dissociation rate.

TRPD is particularly well suited for energy-resolved measurements of slow dissociation processes. [9,10] Traditionally TRPD, which has been developed by Dunbar and co-workers, has employed the Fourier transform ion cyclotron resonance (FTICR) technique for ion trapping and mass spectrometric measurements. In TRPD, ions are produced by an electron ionization pulse or by a laser MPI pulse. They are allowed to relax to their ground state for a preselected time and are then photoexcited by a short laser pulse, and the time-resolved appearance curve of a mass-selected product ion is followed. This can be done for different photon energies provided that the ions absorb in the right wavelength region. Microcanonical rate constants are deduced by this method for time ranges that are impossible to achieve by photoelectron photoion coincidence (PEPICO) methods, namely, in the millisecond range.

The FTICR is not a necessary prerequisite for TRPD measurements and simpler ion trapping devices may suffice. The suitability of our instrumentation, a quadrupole ion trap/reflectron TOF device, for decay time investigations has been demonstrated.[11]

Additional experimental data obtained for a range of photodissociation energies and ion lifetimes will be presented. The conclusions to be presented are based also on RRKM/QET calculations that will be demonstrated to be in good agreement with the experimental observations, indicating that the internal energy, E, is randomized. In other words, under our conditions, these peptides do not circumvent IVR. The possibility that two processes take place in parallel, one that is RRKM-like and another that circumvents IVR will be discussed.

Experimental Section

The Instrument. The experimental apparatus is shown schematically in Figure 1. It consists of three vacuum chambers, for laser desorption, for the quadrupole ion trap, and for a reflectron time-of-flight (TOF) analyzer. The latter two parts have been employed by us and have been described in detail in the past.[11−14] The reflectron TOF mass spectrometer with a quadrupole ion trap (from R. M. Jordan Company) has been developed originally by Lubman and co-workers[15] to combine the storage capabilities of an ion trap with the speed and resolution of a TOF device. The quadrupole ion trap consists of two endcap electrodes and a ring electrode situated between them. The storage capabilities of the device provide enhanced sensitivity and resolution. Resolutions of ∼3500 at m/z 1000 have been quoted.[15b] We have observed resolutions in the range of 500−1000 that are more than adequate for resolving the fragment ions from the parent ion in the LeuTyr and LeuLeuTyr peptides. The goal of our research employing such a combination is similar to that of Neusser's, namely, the observation of

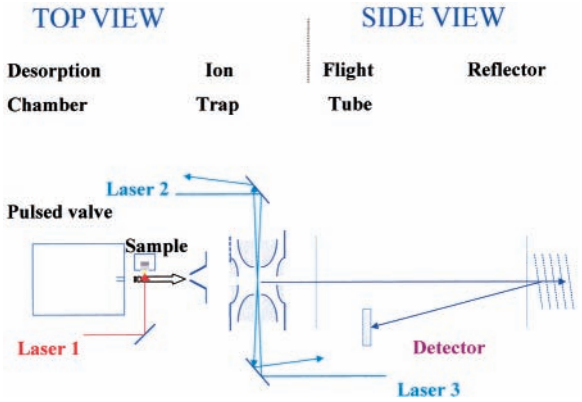

Figure 1. Quadrupole ion trap/reflectron time-of-flight mass spectrometer. Laser no. 1 causes desorption of the peptide sample, laser no. 2 causes ionization, and laser no. 3 causes dissociation.

unimolecular decay of energy-selected ions on the millisecond time scale combined with a fast mass detection process. [16] The device can operate over a wide time range from microseconds to milliseconds.

The first chamber is constructed on axis with the other two. LD followed by jet cooling is carried out in this chamber in a manner similar to the one described by de Vries and coworkers.[17−19] LD of peptides is performed by the 1064 nm fundamental output of a Nd:YAG laser (Minilite from Continuum, 0.5−1 mJ/pulse, 7−10 ns duration), which is focused loosely to a spot on the order of 1.5 mm diameter within 4 mm in front of the nozzle (0.5 mm diameter) of a pulsed supersonic valve (R. M. Jordan Company, 3 bar backing pressure, 4200 A operating current). The quoted stability of the Minilite desorption laser is 2% at 1064 nm. A telescope is used for alignment of the desorption laser spot with respect to the position of the nozzle. A graphite rod covered evenly with the peptide sample is used as a substrate. The sample substrate is moved translationally by a stepping motor to ensure that fresh surface is provided at fixed intervals. There is an effect of the homogeneity of the coverage of the sample on the graphite surface and of the speed of the stepping motor on intensity fluctuations of the LD pulse. The desorbed neutrals are entrained and cooled by collisions with CO_2 or Ar gas through the nozzle. The neutral molecules are introduced into the second chamber downstream through a 3 mm diameter skimmer.

Photoionization and Photodissociation. Photoionization and photodissociation take place in the second chamber where the quadrupole ion trap (a "Paul-trap"[20]) is used as the ion source. The inside surfaces of the trap are hyperbolic. There are six apertures. Two apertures are in the two endcaps, one of which is used as the inlet of the laser-desorbed neutral sample and the other for ion ejection. The extraction hole in the exit endplate has been widened to a 6.35 mm diameter, doubling the original value,[7] to minimize the effect of oscillatory ion intensities caused by laser-induced coherent motion of the ions in the quadrupole trap.[21] Four apertures are in the ring electrode with two at the top and bottom (vertical direction) and the other two in the horizontal direction for the laser beams. About 1 cm above the top aperture is the nozzle of a General Valve pulsed valve that can provide pulsed helium buffer gas.

During operation, the radio frequency (RF) voltage is applied to the ring electrode, while both endcaps are held at 0 V. The RF field serves to trap ions present within the volume of the trap until they are ejected by application of a DC extraction pulse to the exit endcap. During extraction, the RF voltage is turned off. The use of a digital delay generator controls the

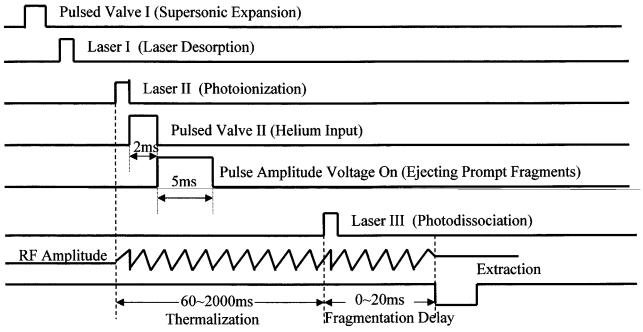

Figure 2. Pulse sequence for the LD/TRPD experiment.

interval that the RF is on from time zero and minimizes the timing jitter so that the storage time does not vary. The initial time delay is from time zero until the RF is triggered off. After a delay of about 2−3 μs to allow for the RF field to disappear, the endcap is dipped in voltage to extract ions from the ion trap. After a typical duration of 2−5 μs for ion extraction, the endcap pulser is turned off and the RF is turned back on. It takes about 100 μs for the RF to come up to the adjusted voltage. The ion trap will continue to store ions until the process is repeated. We have observed in the past[13b] that mass spectra taken for C_{60} between 0 and 1 μs are different. The tail on the C_{60}^+ peak corresponding to delayed ionization was changing dramatically. This indicates that the minimal difference in time delays that results in distinct different experimental rate constants can be as small as 1 μs.

Cold intact neutral molecules undergo two-photon ionization by either one of the following methods: the frequency-doubled output of a dye laser (ND6000, 275−290 nm, 0.3−1 mJ/pulse) pumped by a Nd:YAG laser (Surelite from Continuum) or alternatively the 266 nm fourth harmonic of a Nd:YAG laser (Minilite from NewWave, 0.5 mJ/pulse). Photodissociation is achieved by absorption at various wavelengths in the UV and visible: 289.5 nm, 355 nm, 403 nm, 532 nm, 579 nm, and 630 nm (at 0.2−2.5 mJ/pulse). Both the photoionizing and the photodissociating laser are aligned to pass through the center of the ion trap but from opposite directions (see Figure 1). The photoionizing laser beam is focused, whereas the photodissociating laser beam is out of focus to achieve photodissociation of a greater fraction of the parent ion cloud. The laser power is adjusted by changing the voltage of the pumping YAG laser.

Time-Resolved Photodissociation (TRPD). Two digital delay/pulse generators control all events. Figure 2 shows the timing sequence employed in the measurements. Laser desorption takes place after the opening of the nozzle of the Jordan pulsed valve. The desorbed neutrals are transported into the ion trap where they are photoionized. The pulse to the ionization laser is synchronized with the RF pulse. The storage time of the ions is controlled by another output of the pulse generator by triggering the extraction pulser that serves the dual purposes of ejecting the ions and providing the start-time reference of the TOF mass analysis. The data are collected by a LeCroy Waverunner LT262 digital oscilloscope.

Ionization can produce the parent ions in a variety of excited states. It can also lead to prompt fragmentations. In TRPD, the ionization and excitation steps are separated in time so that the parent ions can undergo radiative and collisional thermalization to lose their excess internal energy acquired in the ionization step. Two additional pulses are applied between the ionization and excitation laser pulses. Pulsed helium buffer gas is provided for the dual purpose of bringing the ions into the center of the trap and enhancing collisional thermalization. This event is

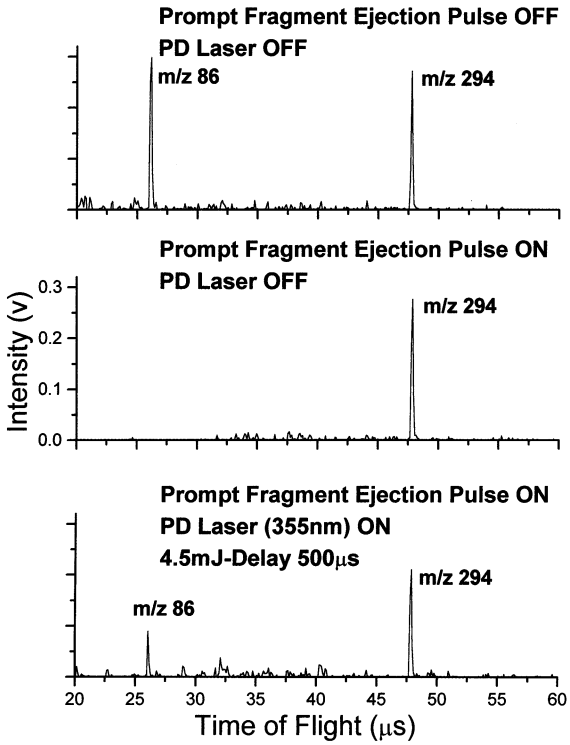

Figure 3. Laser desorption/laser ionization/laser photodissociation mass spectra of LeuTyr. Resonant MPI was at 281.77 nm and photodissociation at 355 nm; see text.

triggered by the second digital delay/pulse generator that is triggered by the Q-switch output of the ionization laser, which makes sure the nozzle opens after the ionization event.[22] The bulk of the helium gas has to be pumped out by the time the excitation laser leading to photodissociation is turned on to ensure that the photoexcited ions undergo no further relaxing collisions. A second pulse serves to eject any prompt fragments that are formed. This is achieved by temporarily increasing the amplitude of the RF voltage that is applied to the ring electrode.[23]

Following thermalization the photoexcitation laser is fired to excite the thermalized ions to well-defined internal energies. This is followed by measurements of the fragment ion buildup as a function of the trapping delay time leading to the TRPD curve. A large number of laser shots is necessary for averaging the results at each time point because of statistical fluctuations, as well as intensity oscillations.[21] Each time point along the TRPD curve is the result of 50−4000 laser shots. Time-dependent daughter ion intensities are normalized via the corresponding parent ion intensities, taking the parent intensity at the shortest trapping time as the reference point, to take into account fluctuations in light intensity for different laser shots and additional pulse fluctuations in the LD process.

The dissociation kinetics of the photoexcited peptide ions can be deduced by exponential fitting of the measured buildup curve of their fragment ions.

Dipeptides and tripeptides were purchased from Sigma (Israel) and were used without further purification.

Results and Discussion

Mass Spectra. The pulsing scheme shown in Figure 2 was tested as before.[7] The mass spectra of LeuTyr were measured under different pulsing conditions as shown in Figure 3. Each of these spectra were measured with the supersonic expansion (pulsed valve I) on, the desorption laser pulse on, the UV photoionization (PI) laser on, and the pulsed helium valve on. The top panel shows a spectrum obtained in a single-color experiment. The photodissociation (PD) laser (III) is turned off and prompt fragments formed by the ionizing laser are not ejected. A relatively high fragmentation yield due to a high ionizing laser power is observed. In the middle panel, the amplitude of the RF voltage that is applied to the ring electrode was temporarily increased. This led to ejection of the unwanted fragments at *m*/*z* 86. In the bottom panel, the RF pulse that leads to ejection of prompt fragments was left on but the PD laser pulse III was turned on. This led to the reappearance of immonium fragment ions at *m*/*z* 86 due to PD of thermalized parent ions at 355 nm. Similar results were observed for the PD of thermalized parent ions of LeuLeuTyr. No additional fragments were observed for either LeuTyr or LeuLeuTyr besides the ion at *m*/*z* 86. We have found the PD yield to scale with the first power of the laser intensity. In other words, the ions at *m*/*z* 86 are the result of a single-photon absorption by the parent ion.

Time-Resolved Photodissociation. In two-color TRPD experiments, two-photon ionization in the UV is followed by one-photon excitation in the UV or in the visible. We have previously demonstrated[7] that thermalization of the parent ions prior to PD is achieved by the helium pulse and by a long thermalization period. The TRPD spectrum obtained for ionization of LeuTyr at 266 nm followed by a thermalization period of 1960 ms and dissociation at 630 nm is presented in Figure 4a. PD is achieved for only a small fraction of the ions, as was also shown to be the case for metal cluster systems,[10] because there is only partial overlap between the ion cloud and the laser beam.[21] Data accumulation is used to improve signal-to-noise ratios. The results of 40 laser shots were accumulated for each time point in a single TRPD curve, and the full TRPD curve was measured in 87 repetitive scans. As a result, each time point is the average of $87 \times 40 = 3480$ laser shots. The rate constant, or inverse time constant, obtained is $k = 360 \pm 100\ s^{-1}$. The process was repeated for lower wavelengths (higher energies). The TRPD spectrum obtained for ionization of LeuTyr at 280.5 nm followed by a thermalization period of 1980 ms and dissociation at 579 nm is presented in Figure 4b. The rate constant, or inverse time constant, obtained for this wavelength is clearly higher, $k = 4800 \pm 1800\ s^{-1}$. Keeping the photoionization and photodissociation energies, as well as the thermalization period, constant but switching to LeuLeuTyr (Figure 4c) leads to a drastic lowering of the rate constant to $k = 290 \pm 190\ s^{-1}$.

Table 1 summarizes selected rate constant data obtained through similar TRPD experiments for LeuTyr and LeuLeuTyr, respectively. Several results transpire: (a) Increasing the thermalization time from nearly 2 s to nearly 4 s has, within experimental error, no effect on the rate constants deduced. The parent ions are already thermalized after 2 s. (b) The experimental rate constants deduced have fairly wide error bars, but within those error limits, separate experiments carried out for the same species and the same PD wavelength yield similar rate constants. (c) The rate constants deduced for the same species (LeuTyr or LeuLeuTyr) at different PD wavelengths are different, increasing with decreasing wavelength (i.e., with increasing energy). (d) The rate constants at the same PD wavelengths are between 1 and 2 orders of magnitude lower for LeuLeuTyr than for LeuTyr. At the same total energy of 2.73 eV (photon energy plus average thermal energy, see below), the rate constant for LeuLeuTyr is nearly 3 orders of magnitude lower than that for LeuTyr (Table 1).

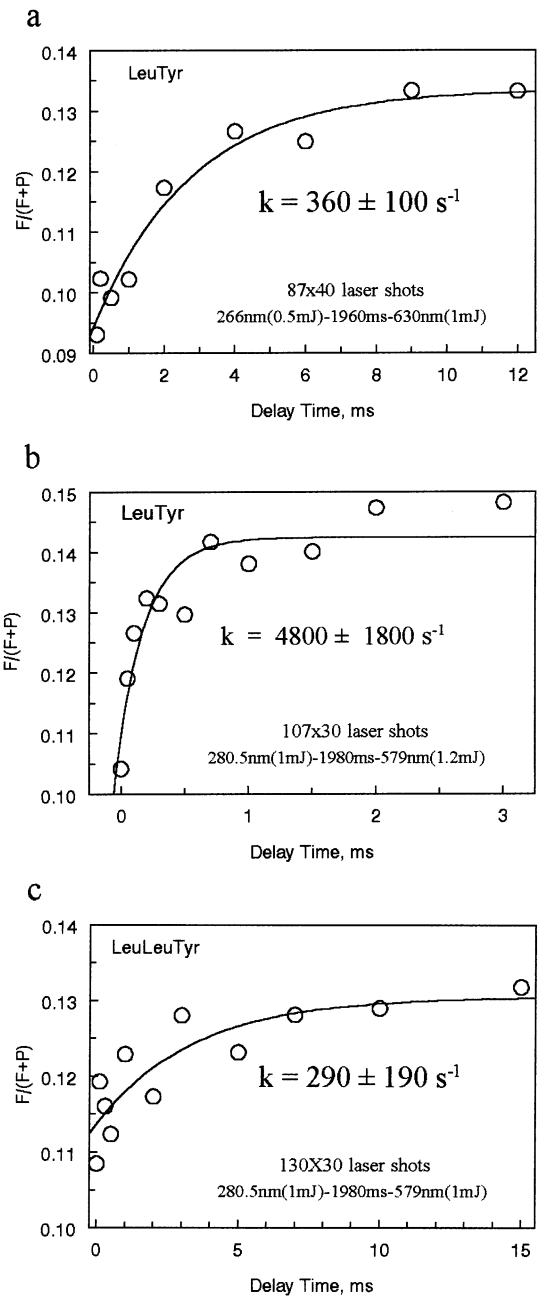

Figure 4. Normalized signals of the immonium ion with increasing trapping time from the reactions $LeuTyr^{+\bullet}$ (P, *m*/*z* 294) → $immonium^+$ (F, *m*/*z* 86) in the dipeptide leucyl tyrosine and $LeuLeuTyr^{+\bullet}$ (P, *m*/*z* 407) → $immonium^+$ (F, *m*/*z* 86) in the tripeptide leucyl leucyl tyrosine: (a) one-color (266 nm, 0.5 mJ), two-photon ionization, thermalization for 1960 ms, and excitation at 630 nm (1 mJ) of LeuTyr; (b) one-color (280.5 nm), two-photon ionization, thermalization for 1980 ms, and excitation at 579 nm of LeuTyr; (c) one-color (280.5 nm), two-photon ionization, thermalization for 1980 ms, and excitation at 579 nm of LeuLeuTyr. Photoionization is followed by collisional cooling with a helium pulse and by a pulse to the ring electrode that temporarily increases the amplitude of the RF voltage to eject fragment ions formed in the ionization pulse. A total thermalization period of nearly 2 s is applied before the photodissociation pulse is turned on. The experimental points are fitted with single-exponential curves (solid lines) yielding inverse time constants (i.e., rate constants): (a) $(3.6 \pm 1) \times 10^2\ s^{-1}$; (b) $(4.8 \pm 1.8) \times 10^3\ s^{-1}$; (c) $(2.9 \pm 1.9) \times 10^2\ s^{-1}$.

Results c and d demonstrate that these peptides do not circumvent IVR under our experimental conditions. The very different rate constants for LeuTyr and LeuLeuTyr provide a clear indication that the peptide length (i.e., its number of degrees of freedom) strongly correlates with the dissociation rate. The assumption that the entire available internal energy *E* is distributed over all of the degrees of freedom is seen to be correct. This point will be checked further below by comparison of RRKM/QET calculated rate constants with the experimental values of Table 1.

Quantum Chemical and RRKM/QET Calculations. Several attempts have been made[24,25] at RRKM calculations for large polypeptide ions. One problem is the lack of knowledge concerning the vibrational frequencies required for calculations of densities of vibrational states. When relatively small peptides are of interest, as is the case here, AM1 calculations of vibrational frequencies suffice.[26] Higher-level DFT calculations are also plausible. A more severe problem is the question how to treat the large number of conformers that have very closely spaced energetics. This question has not yet been fully addressed.[27] An equilibrated mixture of isomers slows down the reaction because the additional potential energy wells add to the density of states of the reactant.[28]

Quantum chemical calculations were carried out using the Gaussian suite of programs.[29] About 25 different initial structures were tried for $LeuTyr^{+\bullet}$ and $LeuLeuTyr^{+\bullet}$, representing different backbone and side-chain conformations. The most stable $LeuTyr^{+\bullet}$ and $LeuLeuTyr^{+\bullet}$ conformers were deduced from geometry optimizations at the AM1 level of theory. Vibrational frequencies were computed also at the AM1 level and scaled by 0.9532. For $LeuTyr^{+\bullet}$, the four most stable conformers and a fifth that is higher in energy at the AM1 level but was suspected to be a low-energy species with DFT have been further subjected to single-point B3LYP calculations on the AM1 geometries. The results confirmed the identity of the lowest-energy conformer. There are additional low-energy conformers that can be obtained mainly by changing side-chain dihedral angles. Others are zwitterionic insofar as the amine terminus is protonated and carries a large fraction of the charge. Contrary to the $LeuTyr^{+\bullet}$ conformers, which are open-chain ones, low-energy $LeuLeuTyr^{+\bullet}$ backbone conformers are folded. Within a narrow energy range above the most stable conformer, there are many more conformers for $LeuLeuTyr^{+\bullet}$ than for $LeuTyr^{+\bullet}$. Whereas we did not attempt to carry out a full conformer search, we are certain about the identity of the lowest-energy species for $LeuTyr^{+\bullet}$ and $LeuLeuTyr^{+\bullet}$.

DFT frequencies were calculated for the lowest-energy conformers. The DFT method used is B3LYP; the basis set used is 6-31+G** for all N and O atoms and all H atoms bonded to O or N, as well as the H atoms on the tyrosine side-chain ring. The basis set used for the rest of the atoms is 6-31G*. The AM1 and DFT geometries are somewhat different in that the interaction of the Tyr side chain with the backbone O atoms is less-favored with DFT. The frequencies computed with both methods agree for some vibrations but are very different for some others.

Microcanonical rate constants, $k(E)$ were calculated according to

$$k(E) = \frac{\sigma N^{\ddagger}(E - E_0)}{h\rho(E)} \qquad (1)$$

where $\rho(E)$ is the density of vibrational states at the energy E, E_0 is the critical energy of activation, $N^{\ddagger}(E - E_0)$ is the sum of the vibrational states from 0 to $E - E_0$ in the transition state, h is Planck's constant, and σ is the reaction path degeneracy factor. The microcanonical rate coefficient $k(E)$ is calculated as a function of energy by an RRKM program.[28,30] The first trial

TABLE 1: Summary of Experimental Rate Constants by TRPD

sample	PI (nm, mJ)	thermalization time (ms), laser repetition rate (Hz)	PD (nm, mJ)	laser shots per time point	energy, eV[a]	k (s^{-1})
LeuTyr	266, 0.5	1980, 0.5	532, 0.5	2200	2.73	$(1.6 \pm 1.1) \times 10^5$
	266, 0.5	1980, 0.5	579, 2.5	200	2.54	$(7.1 \pm 4.4) \times 10^3$
	266, 0.5	1960, 0.5	630, 1	3500	2.37	$(3.6 \pm 1.0) \times 10^2$
	266, 0.5	1980, 0.5	579, 2.5	50	2.54	$(8.7 \pm 2.5) \times 10^3$
	280.5, 1	1980, 0.5	579, 1.2	3000	2.54	$(4.3 \pm 1.6) \times 10^3$
	280.5, 1	3980, 0.25	579, 1	1000	2.54	$(5.0 \pm 2.1) \times 10^3$
LeuLeuTyr	266, 0.5	1980, 0.5	403, 0.2	720	3.67	$(5.1 \pm 4.4) \times 10^4$
	266, 0.5	1980, 0.5	532, 1	1500	2.92	$(1.9 \pm 1.6) \times 10^3$
	266, 0.5	1980, 0.5	579, 1	3900	2.73	$(2.9 \pm 1.9) \times 10^2$

[a] Photodissociation energy plus average thermal energy. The thermal energy distributions of Figure 6 served to calculate the average thermal energies of $LeuTyr^{+}$ and $LeuLeuTyr^{+}$, respectively that were added to the photon energy in the PD step in order to deduce the ion energies.

value for the activation energy of the $LeuTyr^{+\bullet}$ and $LeuLeuTyr^{+\bullet}$ reaction, the cleavage α to the amine terminus leading to the immonium ion *m*/*z* 86, was taken to be $E_0 = 1.5$ eV based on the value of Weinkauf et al.[8a] It is well accepted that RRKM calculations are not sensitive to the details of vibrational frequencies of the molecular ion and transition state but rather to the relative change in frequencies along the reaction coordinate characterized by the activation entropy, $\Delta S^{\dagger}$.[31] The activation entropy does not appear as such in eq 1, but the frequencies that define the degree of looseness of the transition state affect both $\Delta S^{\dagger}$ and $k(E)$. We have adopted E_0 and $\Delta S^{\dagger}$ as parameters. Because LeuTyr and LeuLeuTyr undergo the same cleavage, the pair E_0 and $\Delta S^{\dagger}$ was taken to be equal for the two reaction systems. In the present calculations, the molecular frequencies of the reactant were either the AM1 or the DFT frequencies for the most stable conformer. Those of the transition state were equal to the reactant frequencies except for one frequency, ~990 cm^{-1}, that is the reaction coordinate and was deleted in the transition state. Six additional frequencies of the reactant, in the range 100−700 cm^{-1}, were varied together to the same final value in the transition state so that the desired looseness was achieved. The activation entropy that gave the best fit to the data was calculated on the basis of these changes in frequencies. The reaction path degeneracy, σ, was taken to be 1. Computations could be made more elaborate in the future by taking additional conformers into account. The ones calculated by the quantum chemical methods all lie considerably lower than the dissociation limit although isomerization barriers have not been calculated. As a result, the added density-of-states terms for the different conformers[28] in the denominator of eq 1 are partly or fully offset by a higher σ value provided each of these conformers reacts separately to give the immonium ion.

Computed rate−energy, $k(E)$, dependencies are compared in Figure 5 with the experimental results presented in Table 1. The vertical error bars are those from Table 1. Horizontal error bars are between approximately ±0.4 eV (for LeuTyr) and approximately ±0.6 eV (for LeuLeuTyr); an error bar is shown in Figure 5 for one of the LeuTyr points. The horizontal error bars are due to the widths of the thermal energy distributions of the ions at room temperature. Whereas the absolute error in the internal energy can be quite large, the relative error, which is more important, is much smaller. We have computed the thermal energy distributions from the vibrational frequencies, and they are presented in Figure 6. The thermal distributions and the $k(E)$ dependencies calculated were found to be insensitive to the set of vibrational frequencies chosen for the reactant ions, whether AM1 or DFT.

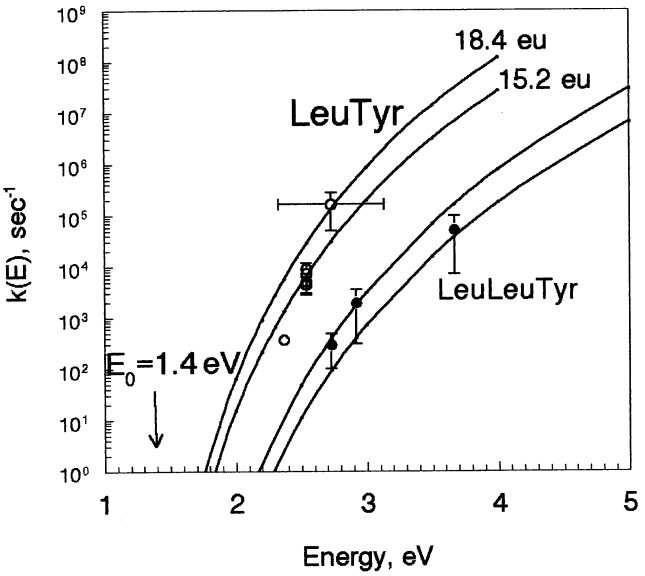

Figure 5. Microcanonical rate−energy dependencies for the reactions producing the immonium ion from $LeuTyr^{+\bullet}$ and $LeuLeuTyr^{+\bullet}$. The rate constant $k(E)$ is plotted on a logarithmic scale as a function of internal energy E in the reactant ion. The open circles (for LeuTyr), filled circles (for LeuLeuTyr), and error bars are experimental data, and the lines are calculated using RRKM/QET and a model with $E_0 = 1.4$ eV and $\Delta S^{\dagger} = 15.2-18.4$ eu. The horizontal error bar shown for one LeuTyr point demonstrates the width of the thermal energy distribution.

The experimental $k(E)$ data can be reproduced fairly well (within somewhat large error limits) by the RRKM calculations (Figure 5). The model that fits the data is $E_0 = 1.4$ eV and $15.2 \leq \Delta S^{\dagger} \leq 18.4$ eu. The E_0 found as a fit is very nearly equal to the value of Weinkauf et al.[8a] The Arrhenius preexponential, A, factor calculated from $\Delta S^{\dagger}$ is at 1000 K $1 \times 10^{17} \leq A \leq 6.2 \times 10^{17}$ s^{-1}. The transition state is quite loose with a high positive activation entropy and high A factor. Further ab initio calculations may be done to verify this point. Williams and coworkers[32] have observed some quite loose transition states for cleavages of the amide backbone in multiply protonated proteins and peptides when using the blackbody infrared dissociation (BIRD) technique. Very high Arrhenius preexponential A factors (up to 10^{39} s^{-1}) were found for the dissociation of large gaseous multiprotein complexes. [33]

Conclusion

We have demonstrated for the peptides LeuTyr and LeuLeuTyr that the observed dissociation of the corresponding cation

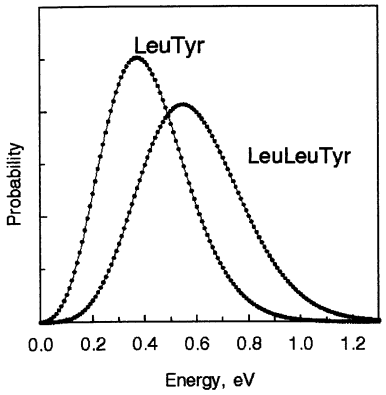

Figure 6. Thermal energy distributions for $LeuTyr^{+\bullet}$ and $LeuLeuTyr^{+\bullet}$ at 300 K. The integrated probabilities are normalized to one. These distributions served to calculate the average thermal energies of $LeuTyr^{+\bullet}$ and $LeuLeuTyr^{+\bullet}$ that were added to the photon energy in the PD step to deduce the ion energies given in Table 1 and in Figure 5.

radicals correlates with peptide length, that is, with the number of degrees of freedom or the number of atoms. Furthermore, the experimental microcanonical rate−energy dependencies, $k(E)$, that span a range of about 3 orders of magnitude can be reproduced by RRKM/QET calculations. In other words, under our conditions these peptides do not circumvent IVR. Electronic excitation (or the charge) may be the scout because charge transfer is a very fast and efficient process,[8b] but the pitfall of large molecule kinetics is not avoided, and we do not observe charge-directed reactivity. The charge only directs the dissociation insofar as α cleavage is the preferred low-energy dissociation route of amine cation radicals leading to the immonium ion (Scheme 1).[34]

It may be claimed that comparison of our data taken on the millisecond time scale with those taken on the microsecond time scale[8] is pointless because of the large difference in time scales and completely different relaxation mechanisms that prevail. The two experiments may be regarded as complementary. However, if the mechanism by which the pitfall of large molecule kinetics is avoided[8] were to prevail, then there should be no dissociations on the millisecond time scale and we could not have observed them. One distinct advantage of the present experiment is the measurement of rate constants that are a much more basic attribute than mass spectra. Furthermore, we were able to span a fairly wide range of rate constants, from $\sim 10^2$ to $\sim 10^5$ s^{-1}.

The TRPD curves (Figure 4) have finite intercepts at zero delay times. This indicates a contribution from a reaction component that is fast on the time scale of the present experiments. Could this be the charge-directed dissociation that avoids IVR? The possibility cannot completely be ruled out, in which case we might have RRKM-like behavior together with a non-RRKM component. However, such nonzero intercepts are well-known from previous TRPD work[9] to be due to multiphoton dissociation processes. In other words, whereas the TRPD curve is due to a single-photon dissociation, the intercept is due to a much faster two-photon dissociation but one that is still within the domain of RRKM.

According to Weinkauf et al.,[8a] the $LeuLeuTyr^{+\bullet}$ cation radical does not dissociate upon absorption of a visible photon in the wavelength range 520−560 nm. A single photon cannot lead to dissociation because the energy is too low (2.2−2.4 eV, not including thermal energies). The first photon energy absorbed causes charge migration out of the aromatic chromophore, and a second photon cannot be absorbed. Our experiments that do demonstrate dissociation in this wavelength region show that it is all a question of time scales. The very short time scale of the original experiments (microseconds) cannot detect dissociations the natural rates of which are in the millisecond time range.

The mode of preparation of excited ions may be critical from the point of view of IVR. Neutral tyrosine-containing dipeptides, including LeuTyr, absorb at about 280.5−281.75 nm because of the aromatic chromophore, and that is where they can be resonantly ionized.[8a,18,35] The ionization process can be "soft" leading to no fragmentation. The ions absorb in the green in the range of wavelengths 520−560 nm because of the aromatic chromophore, and this is the energy range that has been used in the past[8] to ensure site selectivity in the photoexcitation step. Excitation has been effected in the present experiments not only in the range of wavelengths 520−560 nm but also at 355, 404, 630 nm, etc., that is, with photons that may be absorbed by other parts of the molecular ion besides the aromatic chromophore. Furthermore, in the present method of preparation, the neutral precursors are cold because of the supersonic expansion but the ions that undergo photodissociation are at room temperature and have rather broad thermal energy distributions (Figure 6). The thermal energy may promote IVR once the ion is photoexcited at the chromophore site. The possibility that IVR may be avoided under a different preparation strategy cannot be ruled out. It is possible that the Weinkauf−Schlag group [8] started out with a more well-defined preparation of the initial state that used cold neutrals and soft ionization. On the other hand, most of the analytical work has also been done to date on thermal species with broad energy distributions, and nonstatistical, nonergodic behavior has been claimed to occur.[36]

The large numbers of conformers that exist even for relatively small peptides such as the ones studied here make a very accurate RRKM calculation impossible at present. However, the multiple-well potential surface with the many low-lying isomerization barriers should actually promote IVR because of anharmonic couplings. One way to improve agreement between experiments and RRKM calculations might be to allow for different activation parameters as a function of the peptide chain length. Our fairly large experimental error limits did not warrant this approach at this point, particularly because it would involve introducing additional free parameters.

Some of the peptides studied by Weinkauf et al.[8] have amino acids along the peptide chain that can block the charge transfer from the C-terminus to the N-terminus. We plan to study those peptides next by TRPD. We are also in the process of developing new techniques to study ergodicity for protonated peptides and multiply charged proteins.

Acknowledgment. This research was supported by The Israel Science Foundation founded by the Israel Academy of Sciences and Humanities. The Farkas Research Center is supported by the Minerva Gesellschaft für die Forschung GmbH, München. We thank Dr. Cui, Professor Dunbar, Professor Hase, Dr. Laskin, Professor Levine, Professor Lubman, Dr. Oomens, Professor Schlag, and Professor Weinkauf for very helpful discussions.

References and Notes

(1) Rosenstock, H. M.; Wallenstein, M. B.; Wahrhaftig, A. L.; Eyring, H. *Proc. Natl. Acad. Sci. U.S.A.* **1952**, *38*, 667.

(2) Baer, T.; Hase, W. L. *Unimolecular Reaction Dynamics*; Oxford University Press: New York, 1996.

(3) Lifshitz, C. *Adv. Mass Spectrom.* **1989**, *11*, 713; *Int. J. Mass Spectrom. Ion Processes* **1992**, *118/119*, 315.

(4) Lifshitz, C. *J. Phys. Chem*. **1983**, *87*, 2304.

(5) Grotemeyer, J.; Schlag, E. W. *Acc. Chem. Res*. **1989**, *22*, 399. Zenobi, R. *Int. J. Mass Spectrom. Ion Processes* **1995**, *145*, 51.

(6) Remacle, F.; Levine, R. D.; Ratner, M. A. *Chem. Phys. Lett*. **1998**, 285, 25.

(7) Cui, W.; Hu, Y.; Lifshitz, C. *Eur. Phys. J. D* **2002**, *20*, 565.

(8) (a) Weinkauf, R.; Schanen, P.; Yang, D.; Soukara, S.; Schlag, E. W. *J. Phys. Chem*. **1995**, *99*, 11255. (b) Weinkauf, R.; Schanen, P.; Metsala, A.; Schlag, E. W.; Bürgle, M.; Kessler, H. *J. Phys. Chem.* **1996**, *100*, 18567. (c) Weinkauf, R.; Schlag, E. W.; Martinez, T. J.; Levine, R. D. *J. Phys. Chem. A* **1997**, *101*, 7702.

(9) (a) Dunbar, R. C. *J. Phys. Chem.* **1987**, *91*, 2801. (b) So, H. Y.; Dunbar, R. C. *J. Am. Chem. Soc.* **1988**, *110*, 3080. (c) Dunbar, R. C. *J. Phys. Chem*. **1990**, *94*, 3283. (d) Huang, F. S.; Dunbar, R. C. *J. Am. Chem. Soc.* **1990**, *112*, 8167. (e) Faulk, J. D.; Dunbar, R. C.; *J. Am. Chem. Soc*. **1992**, *114*, 8596. (f) Dunbar, R. C.; Lifshitz, C. *J. Chem. Phys*. **1991**, *94*, 3542 (g) Gotkis, Y. ; Naor, M.; Laskin, J.; Lifshitz, C.; Faulk, J. D.; Dunbar, R. C. *J. Am. Chem. Soc*. **1993**, *115*, 7402. (h) Klippenstein, S. J.; Faulk, J. D.; Dunbar, R. C. *J. Chem. Phys*. **1993**, *98*, 243. (i) Ho, Y.-P.; Dunbar, R. C. *J. Phys. Chem*. **1993**, *97*, 11474. (j) Lin, C. Y.; Dunbar, R. C. *J. Phys. Chem*. **1994**, *98*, 1369.

(10) (a) Walther, C.; Dietrich, G.; Lindinger, M.; Lützenkirchen, K.; Schweikhard, L.; Ziegler, J. *Chem. Phys. Lett.* **1996**, *256*, 77. (b) Lindinger, M.; Dasgupta, K.; Dietrich, G.; Krückeberg, S.; Kuznetsov, S.; Lützenkirchen, K.; Schweikhard, L.; Walther, C.; Ziegler, J. *Z. Phys. D* **1997**, *40*, 347. (c) Schweikhard, L.; Krückeberg, S.; Lützenkirchen, K.; Walther, C. *Eur. Phys. J. D* **1999**, *9*, 15.

(11) Cui, W.; Hadas, B.; Cao, B.; Lifshitz, C. *J. Phys. Chem. A* **2000**, *104*, 6339, 7160.

(12) Weickhardt, C.; Lifshitz, C. *Eur. Mass Spectrom.* **1995**, *1*, 223.

(13) (a) Laskin, J.; Lifshitz, C. *Chem. Phys. Lett.* **1997,** *277*, 564. (b) Laskin J. Ph.D. Thesis, The Hebrew University of Jerusalem, Jerusalem, Israel, 1998.

(14) Laskin, J.; Hadas, B.; Märk, T. D.; Lifshitz C. *Int. J. Mass Spectrom.* **1998**, *177*, L9.

(15) (a) Michael, S. M.; Chien, B. M.; Lubman, D. M. *Rev. Sci. Instrum.* **1992**, *63*, 4277. (b) *Anal. Chem.* **1993**, *65*, 2614.

(16) Grebner, Th. L.; Neusser, H. J. *Int. J. Mass Spectrom.* **1994**, *137*, L1.

(17) Meijer, G.; de Vries, M. S.; Hunziker, H. E.; Wendt, H. R. *Appl. Phys. B* **1990**, *51*, 395.

(18) Cohen, R.; Brauer, B.; Nir, E.; Grace, L.; de Vries, M. S. *J. Phys. Chem. A* **2000**, *104*, 6351.

(19) Nir, E.; Kleinermanns, K.; Grace, L.; de Vries, M. S. *J. Phys. Chem. A* **2001**, *105*, 5106.

(20) Paul, W. *Angew. Chem., Int. Ed. Engl*. **1990**, *29*, 739.

(21) Oomens, J.; Meijer, G.; von Helden, G. *Int. J. Mass Spectrom.* **2002**, *221*, 163.

(22) Williams, T. L.; Stephenson, J. L., Jr.; Yost, R. A. *J. Am. Soc. Mass Spectrom*. **1997**, *8*, 532.

(23) Oomens, J.; Meijer, G.; von Helden, G. *J. Phys. Chem. A* **2001**, *105*, 8302.

(24) Griffin, L. L.; McAdoo, D. J. *J. Am. Soc. Mass Spectrom*. **1993**, *4*, 11.

(25) Derrick, P. J.; Lloyd, P. M.; Christie, J. R. In *Advances in Mass Spectrometry*; Cornides, I., Horváth, G., Vékey, K., Eds.; Wiley: Chichester, U.K., 1995; Vol. 13, pp 23−52.

(26) Laskin, J.; Denisov, E.; Futrell, J. *J. Am. Chem. Soc.* **2000**, *122*, 9703; *Int. J. Mass Spectrom.* **2002**, *219*, 189.

(27) Hase, W. L. Personal communication, 2002.

(28) Baer, T.; Hase, W. L. *Unimolecular Reaction Dynamics; Theory and Experiments*; Oxford University Press: New York, 1996.

(29) Frisch, M. J.; Trucks, G. W.; Schlegel, H. B.; Scuseria, G. E.; Robb, M. A.; Cheeseman, J. R.; Zakrzewski, V. G.; Montgomery, J. A., Jr.; Stratmann, R. E.; Burant, J. C.; Dapprich, S.; Millam, J. M.; Daniels, A. D.; Kudin, K. N.; Strain, M. C.; Farkas, O.; Tomasi, J.; Barone, V.; Cossi, M.; Cammi, R.; Mennucci, B.; Pomelli, C.; Adamo, C.; Clifford, S.; Ochterski, J.; Petersson, G. A.; Ayala, P. Y.; Cui, Q.; Morokuma, K.; Malick, D. K.; Rabuck, A. D.; Raghavachari, K.; Foresman, J. B.; Cioslowski, J.; Ortiz, J. V.; Stefanov, B. B.; Liu, G.; Liashenko, A.; Piskorz, P.; Komaromi, I.; Gomperts, R.; Martin, R. L.; Fox, D. J.; Keith, T.; Al-Laham, M. A.; Peng, C. Y.; Nanayakkara, A.; Gonzalez, C.; Challacombe, M.; Gill, P. M. W.; Johnson, B. G.; Chen, W.; Wong, M. W.; Andres, J. L.; Head-Gordon, M.; Replogle, E. S.; Pople, J. A. *Gaussian 98*, revision A.9; Gaussian, Inc.: Pittsburgh, PA, 1998.

(30) Hase, W. L.; Bunker, D. L. *QCP* **1973**, *11*, 234.

(31) Lifshitz, C. *Adv. Mass Spectrom.* **1989**, *11*, 713.

(32) Price, W. D.; Schnier, P. D.; Jockusch, R. A.; Strittmatter, E. F.; Williams, E. R. *J. Am. Chem. Soc.* **1996**, *118*, 10640.

(33) Felitsyn, N.; Kitova, E. N.; Klassen, J. S. *Anal. Chem.* **2001**, *73*, 4647.

(34) McLafferty, F. W.; Tureček, F. *Interpretation of Mass Spectra*, 4th ed.; University Science Books: Mill Valley, CA, 1993.

(35) Cohen, R. M.Sc. thesis, The Hebrew University of Jerusalem, Jerusalem, Israel, February 2000.

(36) Zubarev, R. A.; Kelleher, N. L.; McLafferty, F. W. *J. Am. Chem. Soc.* **1998**, *120*, 3265. Zubarev, R. A.; Kruger, N. A.; Fridriksson, E. K.; Lewis, M. A.; Horn, D. M.; Carpenter, B. K.; McLafferty, F. W. *J. Am. Chem. Soc.* **1999**, *121*, 2857.